



Nguyen, D. H., Goman, M., Lowenberg, M. H., & Neild, S. A. (2022). Evaluation of Unsteady Aerodynamic Effects in Stall Region for a T-Tail Transport Model. In *AIAA SciTech Forum 2022: AIAA SciTech Forum* [AIAA 2022-1932] American Institute of Aeronautics and Astronautics Inc. (AIAA). <https://doi.org/10.2514/6.2022-1932>

Peer reviewed version

Link to published version (if available):  
[10.2514/6.2022-1932](https://doi.org/10.2514/6.2022-1932)

[Link to publication record in Explore Bristol Research](#)  
PDF-document

This is the author accepted manuscript (AAM). The final published version (version of record) is available online via AIAA at <https://doi.org/10.2514/6.2022-1932>. Please refer to any applicable terms of use of the publisher.

## University of Bristol - Explore Bristol Research

### General rights

This document is made available in accordance with publisher policies. Please cite only the published version using the reference above. Full terms of use are available: <http://www.bristol.ac.uk/red/research-policy/pure/user-guides/ebr-terms/>

# Evaluation of Unsteady Aerodynamic Effects in Stall Region for a T-Tail Transport Model

Duc H. Nguyen<sup>1</sup>

*University of Bristol, Bristol, BS8 1TR, United Kingdom*

Mikhail G. Goman<sup>2</sup>

*De Montfort University, Leicester, LE1 9BH, United Kingdom*

Mark H. Lowenberg<sup>3</sup> and Simon A. Neild<sup>4</sup>

*University of Bristol, Bristol, BS8 1TR, United Kingdom*

**Although quasi-steady aerodynamic modelling is a widely used technique, its shortcomings in representing the stall and post-stall dynamics have been noted in the literature. Various methods to model the unsteady aerodynamics effects have been proposed as a result, but their direct implications on the aircraft's flight dynamics characteristics have not been widely studied. In this paper, we combine the state-space method for unsteady aerodynamic modelling with bifurcation analysis to examine the sensitivity of stall and post-stall behaviour to the choice of aerodynamic modelling method: quasi-steady or unsteady. It is found that quasi-steady modelling is adequate for the chosen example of a T-tailed transport aircraft that does not undergo rapid manoeuvring. The study is then expanded to investigate a hypothetical situation with highly unsteady aerodynamic characteristics resembling a delta wing configuration – achieved by increasing the time delay constants in the unsteady model. This results in an aircraft with significantly lower flying qualities as indicated by bifurcation analysis. These findings highlight the need to implement unsteady aerodynamic modelling techniques in high-performance aircraft with significant vortex-related unsteady aerodynamics in order to sufficiently capture their stall and post-stall dynamics.**

## I. Introduction

Representation of aerodynamic forces and moments in flight dynamics is traditionally based on the use of stability and control derivatives, which can adequately model the dynamics at low angles-of-attack during normal flights [1]. Nevertheless, it has been noted that the stall and post-stall dynamics require special formulations of aerodynamic characteristics to ensure an increase in the manoeuvrability of a combat aircraft and the safety of a transport aircraft in situations of loss of control in-flight (LOC-I) [2, 3]. In the stall region, aerodynamic forces and moments are not only nonlinear but also exhibit noticeable unsteady effects during the transient motion of the aircraft. The use of multi-dimensional data tables – obtained from static and dynamic wind tunnel tests, CFD or ultimately from flight tests – can capture the static nonlinearities well. However, the inclusion of unsteady (time-dependent) phenomena arising from testing or simulating under transient conditions is not well-established, especially in the stall and post-stall regions. It is now recognised that there is a need to adequately account for time-dependent flow phenomena in models in both military and civil applications [4-6]. On highly-maneuvrable applications, unsteady effects can lead to strong discrepancies between the behaviours predicted using best-practice wind-tunnel tests and actual test flights [7]. Similarly, adequate modelling of unsteady aerodynamics of a transport airplane in the stall region with a massive flow

---

<sup>1</sup> PhD Student, Department of Aerospace Engineering. Student Member AIAA.

<sup>2</sup> Professor of Dynamics, School of Engineering and Sustainable Development. Senior Member AIAA.

<sup>3</sup> Professor of Flight Dynamics, Department of Aerospace Engineering. Senior Member AIAA.

<sup>4</sup> Professor of Nonlinear Structural Dynamics, Department of Aerospace Engineering.

separation is critical for flight simulation and pilot training in situations involving upsets and loss-of-control in flight (LOC-I) [3].

Even when a suitable unsteady aerodynamic model has been established, there remains the challenge of assessing the stability and control characteristics of the aircraft model for both steady-state and transient/perturbed conditions in the presence of these time-dependent phenomena. This is not a straightforward task. While steady-state study may suggest that the nonlinear system is stable, instabilities and counter-intuitive behaviour can still be found under transient conditions. This gives further impetus to establish a means of capturing such phenomena mathematically and then to assess their implications on the aircraft's flying qualities.

One of the common methods for investigating nonlinearities in flight dynamics is bifurcation analysis. Since its first application in the early 80s [8, 9], the method has been recognised by both researchers and the industry for its capability of characterising many important phenomena encountered at high angles-of-attack and sideslip, such as spin, wing rock, and static hysteresis. This makes bifurcation analysis a popular choice for studying the behaviours of high-performance fighter jets [10, 11] as well as transport aircraft in upsets and loss-of-control situations [12, 13]. It has also been used for the study of rotorcraft, where the periodic nature of rotor behaviour in forward flight are facilitated via the use of harmonic forcing [14]. Recent works have extended this form of bifurcation analysis to assess the flight dynamics of fixed-wing aircraft under an external harmonic forcing term [15, 16]. Referred to as 'nonlinear frequency analysis' or 'harmonically-forced bifurcation analysis', this approach permits the construction of a Bode plot without relying on linearisation and transfer functions – therefore allowing the non-stationary nonlinear effects such as sub- and super-harmonic resonance [15] and actuator rate limiting [16] to be directly reflected in the frequency response. In the context of unsteady aerodynamic analysis, nonlinear frequency response is an especially suitable tool because a harmonically-forced aircraft is non-stationary by nature, meaning that the time-dependent aerodynamic effects observed during the aircraft's transient motion can be directly reflected in the analysis. As a result, the insights gained by nonlinear frequency analysis cannot be obtained from linear-based methods or conventional (unforced) bifurcation analysis due to their linear and stationary nature, respectively.

As mathematical models that incorporate unsteady aerodynamics become more widespread, so does the need to systematically assess the capability of this new modelling method comparing to the conventional quasi-steady approach. To initiate work on the topic, this paper considers the longitudinal dynamics of the NASA GTT (Generic T-tail Transport) airliner model. We use both conventional bifurcation analysis and the nonlinear frequency response to examine the sensitivity of stall and post-stall behaviours to the choice of unsteady modelling method: quasi-steady or unsteady. The GTT uses wind tunnel test data by NASA and Boeing [17-19] from both static and forced oscillation tests, resulting in a nonlinear but conventional (quasi-steady) flight dynamics model. We then augment the quasi-steady GTT model with unsteady aerodynamics effects using the state-space method (sometimes referred to as the Goman-Khrabrov model in the literature) [4], so as to compare the two aerodynamic modelling techniques and validate the capability of the state-space approach in matching the forced oscillation test results. Finally, the study is expanded to consider a hypothetical highly-unsteady version of the GTT by artificially increasing the magnitude of delay-relaxation parameters to the values typical of a delta wing configuration [6]. This is done to demonstrate the advantages of our proposed approach to the study of transient dynamics while also providing a speculative study on the impacts of strong unsteady effects in terms of flight dynamics and control.

## II. Modelling and Validation

The first mathematical formulation of the aeroplane's longitudinal dynamics was introduced in 1911 by Bryan, where the aerodynamic derivatives in the equations of motion were treated as constant coefficients [1]. This was later expanded to accommodate flights at different conditions by turning these coefficients into functions of the angles of attack (and often other states such as speed or Mach number, and of control surface deflections), thereby creating the so-called quasi-steady modelling method. Despite its role as the foundation for modern flight dynamics and control analyses [2], it is known that quasi-steady method cannot accurately model the unsteady aerodynamic effects in the stall region, such as delayed flow attachment and separation. In these instances, the state-space aerodynamic modelling method has been shown to be a better way to reflect these phenomena [4]. The formulation and implication of both approaches are discussed in this section.

### A. Quasi-Steady Modelling

As mentioned, the aerodynamic coefficients in the quasi-steady approach are functions of the angle of attack. Their nonlinear relationships are usually measured in wind tunnel static tests or predicted computationally, in either case keeping the angle of attack and sideslip angle constant. The contribution to aerodynamic loads due to the pitch rate  $q$ , rate of change in the angle of attack  $\dot{\alpha}$ , control surface deflections (such as elevator  $\delta_e$ ), is usually considered as a linear increment with an aerodynamic derivative for a given angle of attack. If only the longitudinal motion is considered, the normal force and pitching moment coefficients  $C_z$  and  $C_m$  can be represented in the following form:

$$C_z = C_{z-st}(\alpha) + C_{zq}(\alpha) \frac{qc}{2V} + C_{z\dot{\alpha}}(\alpha) \frac{\dot{\alpha}c}{2V} + C_{z\delta_e}(\alpha) \delta_e \quad (1)$$

$$C_m = C_{m-st}(\alpha) + C_{mq}(\alpha) \frac{qc}{2V} + C_{m\dot{\alpha}}(\alpha) \frac{\dot{\alpha}c}{2V} + C_{m\delta_e}(\alpha) \delta_e \quad (2)$$

where the first terms in equations (1) and (2) are the static nonlinear dependencies on the angle-of-attack obtained from static wind tunnel tests, the linear terms representing rotary and unsteady aerodynamic derivatives are normally obtained in wind tunnel forced oscillations tests, while control derivatives are calculated based on linearisation of the experimental nonlinear dependences from static tests. The experimental forced oscillation rigs normally involve pure angular oscillations so that pitch rate  $q$  and the rate of change in angle of attack  $\dot{\alpha}$  are identical. This leads to the measurement of rotary and unsteady aerodynamic derivatives as mixed combinations, for example,  $C_{zq}(\alpha) + C_{z\dot{\alpha}}(\alpha)$  and  $C_{mq}(\alpha) + C_{m\dot{\alpha}}(\alpha)$ . Experimental rigs capable of generating heave motions for separate measurement of these two aerodynamic derivatives exist but are not widely used. As a compromise, representations (1) and (2) are often modified by inclusion of the measured cumulative pairs  $C_{zq}^* = C_{zq}(\alpha) + C_{z\dot{\alpha}}(\alpha)$ ,  $C_{mq}^* = C_{mq}(\alpha) + C_{m\dot{\alpha}}(\alpha)$ , which is partly justified by noting that the changes in airplane stability characteristics due to translational ( $\dot{\alpha}$ ) effects are slight. This results in the following simplified representation:

$$C_z = C_{z-st}(\alpha) + C_{zq}^*(\alpha) \frac{qc}{2V} + C_{z\delta_e}(\alpha) \delta_e \quad (3)$$

$$C_m = C_{m-st}(\alpha) + C_{mq}^*(\alpha) \frac{qc}{2V} + C_{m\delta_e}(\alpha) \delta_e \quad (4)$$

Issues arise when the rotary/unsteady aerodynamic derivatives are measured at stall conditions. This is caused by the flow separation creating a dependency of the measured aerodynamic derivatives on the frequency  $\omega$  and amplitude of forced oscillations:

$$C_z = C_{z-st}(\alpha) + C_{zq}^*(\alpha, \omega) \frac{qc}{2V} + C_{z\delta_e}(\alpha) \delta_e \quad (5)$$

$$C_m = C_{m-st}(\alpha) + C_{mq}^*(\alpha, \omega) \frac{qc}{2V} + C_{m\delta_e}(\alpha) \delta_e \quad (6)$$

It is not possible to directly translate these frequency and amplitude dependencies into time simulation of free flights involving arbitrary motions. This can be partially resolved by replacing the dependence on the frequency  $\omega$  with the dependence on the angular pitching velocity  $q$ , as was done in [17, 19].

## B. State-Space Method for Unsteady Aerodynamic Modelling

The state-space method provides a more accurate representation of the unsteady aerodynamic effect in the normal force coefficient  $C_z$  [4]. Recent development has shown that this approach is successful in modelling the effects of blowing-type plasma actuators for active control of flow separation as well as vertical wind gusts [20, 21]. At its core, the state-space method uses two separate envelope functions  $C_{z-att}(\alpha)$  and  $C_{z-sep}(\alpha)$  to describe the dependencies of attached and fully separated flow on the angle of attack, plus an internal state variable  $x_z$  characterising the delayed transition between  $C_{z-att}(\alpha)$  and  $C_{z-sep}(\alpha)$ . This delay and relaxation process is reflected by a first-order lag in  $x_z$ , which includes two time constants  $T_1$  characterising flow relaxation process and  $T_2$  characterising the delay in flow separation due to the rate of change in angle of attack ( $\dot{\alpha}$ ). Accordingly, the unsteady model for normal force coefficient  $C_z$  can be represented in the following form:

$$C_z = C_{z-att}(\alpha)x_z + C_{z-sep}(\alpha)(1 - x_z) + C_{zq0}(\alpha) \frac{qc}{2V} + C_{z\delta_e}(\alpha) \delta_e \quad (7)$$

$$T_1 \frac{dx_z}{dt} + x_z = x_{z0}(\alpha_{eff}) \quad (8)$$

where:

- $C_{z-att}(\alpha)$  is the dependence of the normal force coefficient assuming that flow is attached
- $C_{z-sep}(\alpha)$  is the dependence of the normal force coefficient assuming that flow is fully separated
- $x_z \in [0,1]$  is a normalised internal state variable characterising transition from attached to separated flow
- $x_{z0}(\alpha)$  is a smooth function describing transition between the attached and separated flow so that  $x_{z0} = 1$  at angles of attack below the stall zone and  $x_{z0} = 0$  at angles of attack above the stall zone
- $T_1$  is physical time in seconds characterising the relaxation process
- $\tau_1 = T_1 V/c$  is the non-dimensional relaxation time
- $\alpha_{eff}$  is the effective angle of attack describing the delay in separation due to the rate of change in angle of attack  $\dot{\alpha}$ ; it can also reflect influence of the Reynolds number  $\Delta Re$  [4] and intensity of jet blowing [20] or vertical wind gust  $w$  [21] when present, i.e.  $\alpha_{eff} = \alpha - T_2 \dot{\alpha} - \Delta \alpha_{Re}$ , where  $\tau_2 = T_2 V/c$  is the non-dimensional time characterising the delay in onset of flow separation
- $C_{zq0}$  is the rotary aerodynamic derivative reflecting contribution from an airframe without account for flow separation on the wing
- $C_{z\delta_e}$  is the aerodynamic control derivative with respect to elevator deflection.

Unsteady aerodynamic modelling in pitching moment is more complicated because the process depends on both the magnitude of the aerodynamic force  $C_z$  and the centre of its application  $x_p$  [5]. Nevertheless, a structure similar to equations (7) and (8) can still be used on a T-tail aircraft because the wing-tail interaction is minimal and hence will not influence the aerodynamic pitching moment in the stall region ( $\alpha$  between  $10^\circ$ - $25^\circ$ ). This is contrary to the conventional (low tail) configuration, where both the development of flow separation on the wing and the delayed action of wing downwash on the horizontal tail must be considered [5]. Accordingly, the contribution to the moment coefficient from flow separation on the wing can be described by a smooth function  $C_{m-ws}(\alpha)$ , which equals zero outside of the stall region, and results in the following unsteady representation of the pitching moment coefficient:

$$C_m = C_{m0}(\alpha) + x_m + C_{mq0}(\alpha) \frac{qc}{2V} + C_{m\delta_e}(\alpha) \delta_e \quad (9)$$

$$T_1 \frac{dx_m}{dt} + x_m = C_{m-ws}(\alpha_{eff}) \quad (10)$$

where:

- $C_{m0}(\alpha)$ ,  $C_{m-ws}(\alpha)$  are the functions describing static dependence of the pitching moment coefficient without account of flow separation over the wing and the contribution from the wing separation to the pitch break, respectively. The sum of these two functions should be equal to the static dependence  $C_{m-st}(\alpha) = C_{m0}(\alpha) + C_{m-ws}(\alpha)$
- $x_m \in [0,1]$  is a normalised internal state variable characterising transition from attached to separated flow
- $C_{mq0}$  is the rotary aerodynamic derivative reflecting contribution from an airframe without account of flow separation on the wing
- $\alpha_{eff}$  is the same effective angle of attack as in equation (8)

Fig. 1a and 1b illustrate the contributions of the static terms in equations (7-8) and (9-10) to the normal force and pitching moment coefficients of the GTT airplane, respectively. The envelope boundaries for the normal force coefficients are quite well approximated as sinusoidal  $C_{z-att}(\alpha) = a \sin \alpha$  and  $C_{z-sep}(\alpha) = b \sin \alpha$ , where  $a = -5.0$ ,  $b = -2.4$ , and  $C_{z0} = -0.27$ . The upper limit  $C_{z-sep}(\alpha) = -5$  is close to the experimental data at small angles of attack below the stall, the lower limit  $C_{z-sep}(\alpha) = -2.4 \sin \alpha$  is close to the experimental data beyond the stall to  $90^\circ$ , while the function  $x_{z0}(\alpha)$  is responsible for the transition between the two envelope functions inside the stall region. The division of the static dependence  $C_{m-st}(\alpha)$  into two components  $C_{m0}(\alpha)$  and  $C_{m-ws}(\alpha)$  was carried out on the basis of engineering judgment. We chose  $C_{m-ws}(\alpha)$  to capture the nonlinear change in pitching moment in the stall region, which is characterised by the onset of an unstable positive slope and subsequent restoration of a negative slope. A similar intuitive judgement can be used for the initial choice of functions  $C_{zq0}(\alpha)$  and  $C_{mq0}(\alpha)$ . This methodology

could be extended to low-tail geometries by considering aerodynamic coefficients for different wing-body-tail, wing-body, and body-tail combinations, obtained from experiments or CFD, supplemented by visualisation of distributed flow parameters.

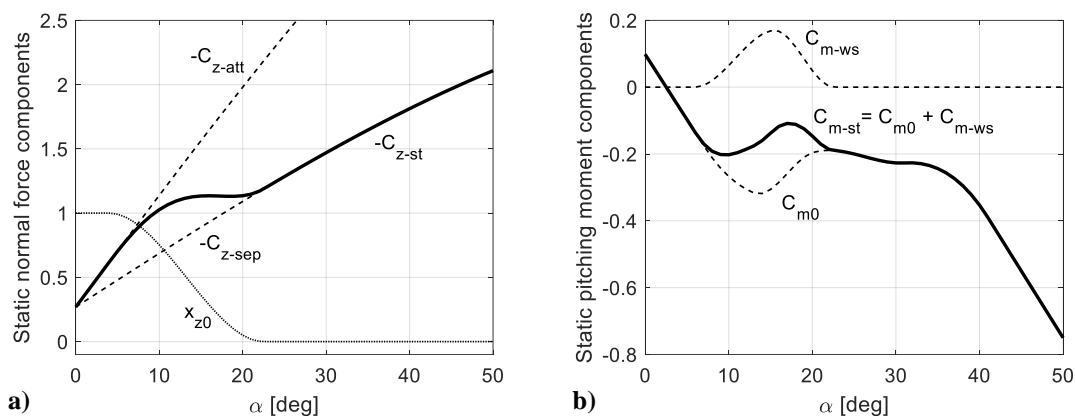


**Fig. 1 Static unsteady aerodynamic components: normal force (a) and pitching moment (b).**

### C. GTT Implementation and Validation

The state-space approach outlined above is now applied to the NASA's Generic T-tail Transport (GTT) model. As the name suggests, the GTT represents a generic mid-size regional jet airliner with a T-tail configuration. Its aerodynamic data were collected from a series of low-speed sub-scale wind tunnel and water tunnel tests, and some preliminary results have been reported in recent conferences [17-19]. Computational fluid dynamics was also deployed to estimate the influence of the Reynolds number on the measured aerodynamics data, allowing the pitching moment and pitch damping data to be adjusted to represent the equivalent full-scale aircraft. For this study, we base our analysis on the original set of data from the sub-scale testing to construct a 4<sup>th</sup>-order model that contains only longitudinal motions while neglecting the horizontal tailplane, flaps and spoilers, which is deemed adequate for this study. All lateral-directional states and inputs are therefore zero. This 4<sup>th</sup>-order implementation contains 19 aerodynamics tables, which are 1D and 3D functions of angle-of-attack and of angle-of-attack/horizontal tailplane/elevator deflections. The valid  $\alpha$  range is from  $-8^\circ$  to  $60^\circ$ .

In order to compare quasi-steady and unsteady aerodynamics modelling techniques, the following three models based on the GTT are created for this study:

- The 'quasi-steady' model is basically the original GTT but with the tabular data for static normal force and pitching moment replaced by spline functions as shown in Fig. 2 (as well as Fig. 1). The use of spline functions instead of lookup tables ensures consistency with the two unsteady models explained below while resulting in negligible difference comparing to the unmodified GTT. This also has the secondary effect of making the model smoother, which is beneficial for bifurcation analysis.
- The 'nominal unsteady model' is augmented with two additional states  $x_z$  and  $x_m$  to describe the internal unsteady dynamics of  $C_z$  and  $C_m$  using the approach outlined in equations (7-10).
- A hypothetical highly-unsteady model is also examined to demonstrate the use of bifurcation analysis in studying unsteady aerodynamics phenomena. In this implementation, the time delay constants are both multiplied by a scale factor of 2.5 (i.e.,  $\tau_1$  and  $\tau_2$  become  $\Lambda\tau_1$  and  $\Lambda\tau_2$ , where  $\Lambda$  equals 2.5). This version is referred to as the ' $\Lambda = 2.5$ ' or 'highly-unsteady' model. Note that  $\Lambda = 1$  is the nominal unsteady model.

It can be seen from Fig. 2 that the spline functions demonstrate an acceptable level of agreement between experimental and modelling results for static dependencies. To verify the dynamic dependencies, the damping derivatives  $C_{zq}^*(\alpha)$  and  $C_{mq}^*(\alpha)$  of the quasi-steady and nominal unsteady models are now compared in Fig. 3. The simulation condition used to obtain these derivatives was selected to match the amplitude and frequency of angle-of-attack oscillations during wind tunnel experiments [18]:  $5^\circ$  in amplitude, 0.44 Hz in frequency at  $Re = 230,000$  and flow speed  $V = 18$

m/s. Correct identification of  $\tau_1$  and  $\tau_2$  should result in an unsteady model with damping derivatives  $C_{zq}^*(\alpha)$  and  $C_{mq}^*(\alpha)$  matching experimental data (quasi-steady modelling) in the condition specified above, especially in the stall region. The tuning process was done empirically, giving  $\tau_1 = 4.5$  and  $\tau_2 = 3.5$  for a reasonably good match. A more comprehensive approach would involve calculating  $\tau_1$  and  $\tau_2$  using a formal identification method to ensure the best fit between experimental and modelling result [6, 22], but this is beyond the scope of the paper.

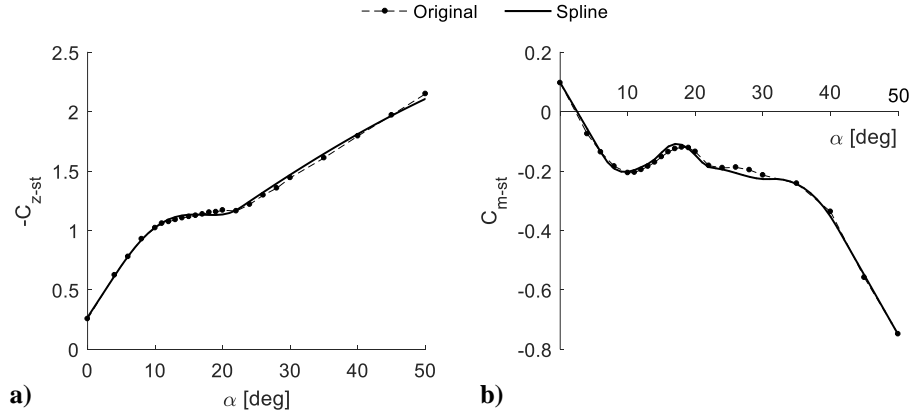


**Fig. 2 Fitting of the static aerodynamic coefficients.**

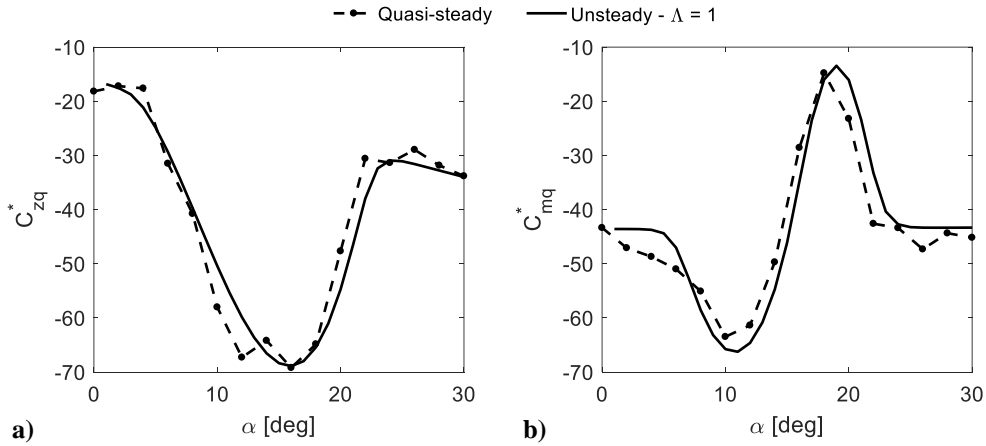


**Fig. 3 Out-of-phase aerodynamic derivatives  $C_{zq}^*$  and  $C_{mq}^*$  from NASA wind tunnel tests [18] and simulated using the nominal unsteady aerodynamic model, obtained at frequency 0.44 Hz and amplitude 5°.**

It is worth noting that the values of  $\tau_1$  and  $\tau_2$  are similar to those obtained in [17] based on CFD simulations of the NASA Common Research Model (CRM) wing-body configuration. The aerodynamic model structure for the normal force coefficient in [17] was identical to (7-8) and the considered wing-body configuration excludes the interference with the horizontal tail. The dimensionless time constants found in [14] for this case were  $\tau_1 = 4.86$  and  $\tau_2 = 3.89$ . These values are very close to those obtained in this study for the GTT aircraft, based on the NASA wind tunnel test data [18] and utilising the aerodynamic models (7-8) and (9-10), namely  $\tau_1 = 4.5$  and  $\tau_2 = 3.5$ . This provides a reasonable independent verification of the obtained time constants in our study. Additionally, the time scale for the model of the normal force coefficient of the wing-body-tail configuration in [17] shows an increase in the relaxation time  $\tau_1 = 7.77$  and no change in the delay  $\tau_2 = 3.89$ . This increase in relaxation time  $\tau_1$  can be justified as it now includes additional time for the downwash of the wing to act on the horizontal tail.

Aerodynamic derivatives obtained from forced oscillation tests in a wind tunnel in a stall region usually depend on the frequency and amplitude of the oscillations. To illustrate such dependencies in the normal force and the pitching moment coefficients, Fig. 4 shows the estimated traditional rotary aerodynamic derivatives (3-4) for the GTT aircraft

obtained as an out-of-phase aerodynamic derivative from simulated forced oscillation tests using the identified unsteady aerodynamic models (7-8) and (9-10). The peaks of the derivatives  $C_{zq}^*(\alpha)$  and  $C_{mq}^*(\alpha)$  in the stall region decrease with increasing frequency  $\omega$ , demonstrating a significant dependence on frequency. Such dependence on frequency makes the use of the quasi-steady aerodynamic model (3-4) problematic for simulations in the time domain in the stall region. The increase of frequency correlates with the increase of pitch rate amplitude  $q_{max}$  during forced oscillations executed at the same amplitude. This is why in [17, 19], for example, the damping terms are the equivalent of equations (5-6), where frequency was replaced with angular rate  $q$ . Such modification of the quasi-steady aerodynamic model allows only the delay process in flow separation to be represented, while the relaxation process is not accounted for. The relaxation process is important in modelling of a vertical wind gust effect in the stall region. In equations (7-10), the gust effect can be incorporated in the effective angle of attack as follows:  $\alpha_{eff} = \alpha - (\tau_2 c/V)\dot{\alpha} - \Delta\alpha_{Re} + \alpha_w - (\tau_2 c/V)\dot{\alpha}_w$ , where  $\alpha_w$  is the change in angle of attack generated by the vertical gust [21].

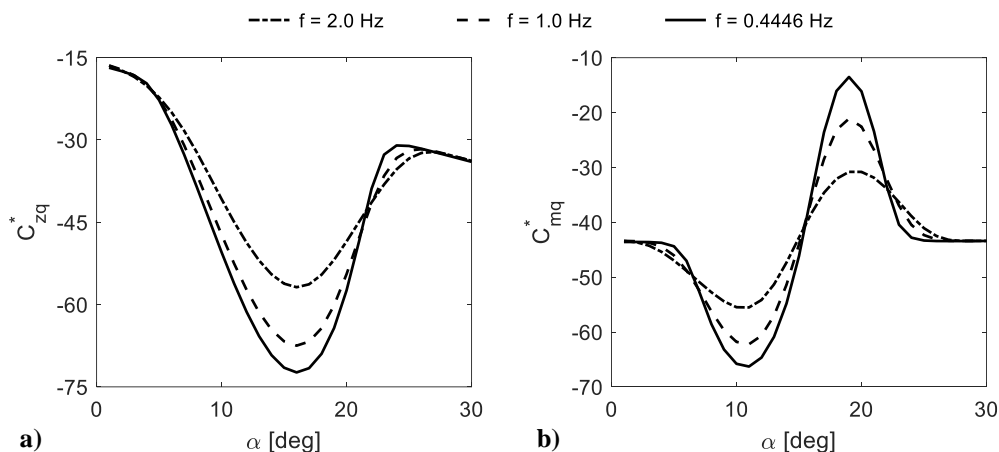


**Fig. 4 Out-of-phase aerodynamic derivatives  $C_{zq}^*$  and  $C_{mq}^*$  of the unsteady models – obtained in simulated forced pitch oscillations with amplitude  $5^\circ$  and different frequencies.**

Now that the unsteady model has been verified to show a good match to the static and quasi-steady data under equivalent conditions, the effects of increasing the unsteady effects via the scaling factor  $\Lambda$  are examined. Fig. 5 compares the quasi-steady and unsteady force and moment coefficients when the angle-of-attack is subjected to a sinusoidal forcing. It can be observed that a good match is achieved between the quasi-steady and nominal-unsteady model. In fact, the unsteady effects only become more prominent by increasing  $\Lambda$  to 2.5, resulting in the differences seen around the stall region of the highly-unsteady model. Specifically, negative damping results in the twisted  $C_M$  loop of the  $\Lambda = 2.5$  response as well as a thicker  $C_Z$  loop, which are indicative of more unsteady dynamics due to the increased delay in flow separation and reattachment. The choice of  $\Lambda = 2.5$  in this study can be regarded as representative of a configuration in which the unsteady effects play a bigger role. For reference, the equivalent scaling factor in the case of the delta wing study in [6] is approximately  $\Lambda = 3.4$ .

It has been shown that the state-space method is a feasible alternative to the quasi-steady approach because their responses are more or less the same in regions where the quasi-steady data is known to be valid (i.e., for forced oscillation conditions equivalent to those used in the wind tunnel tests from which the quasi-steady dynamic derivatives were defined). Furthermore, a modification to the time delay constants using the scaling factor  $\Lambda$  brings out the unsteady aerodynamics effects of interest for an aircraft configuration in which there are stronger time dependencies; this facilitates a speculative study on the potential ramifications of unsteady effects on the aircraft's dynamics. These three models are now implemented on the fourth-order equations of motion to create the corresponding longitudinal flight dynamics models with four states  $[\alpha, V, q, \theta]$  (plus two additional states  $x_z$  and  $x_m$  for the unsteady versions), which will be studied using bifurcation analysis in the sections to follow.



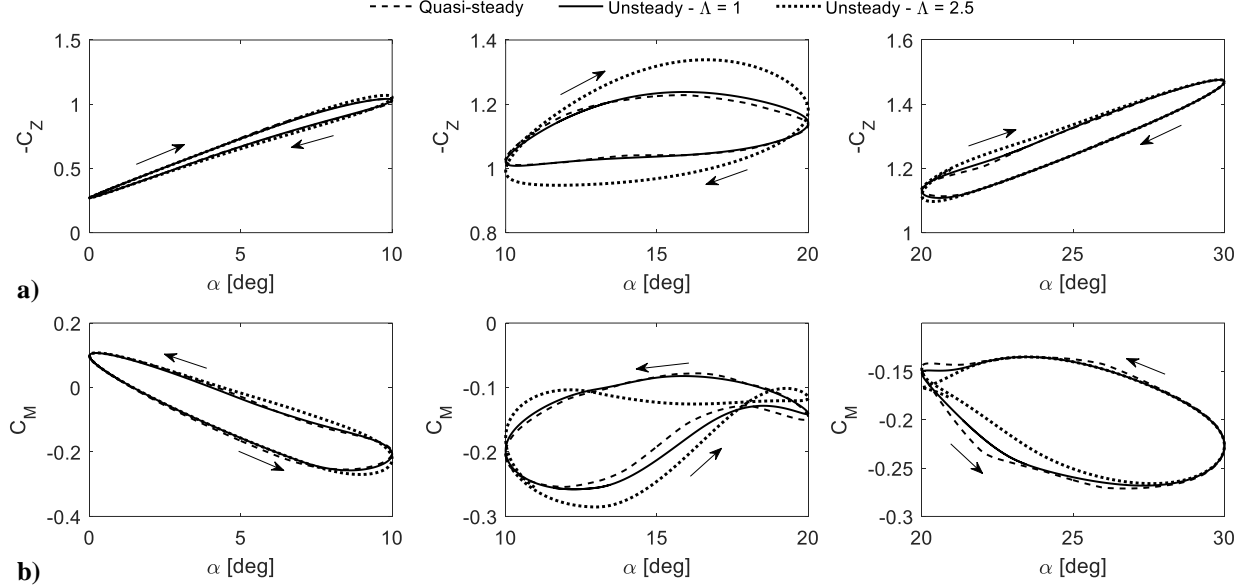


**Fig. 5 Normal force (a) and pitching moment (b) variation in a sinusoidal  $\alpha$  forcing at 0.4446 Hz and 5° amplitude – quasi-steady vs unsteady.**

### III. Bifurcation Analysis

The basics of bifurcation methods are illustrated in this section. For a comprehensive introduction to the topic, readers are referred to nonlinear dynamics textbooks such as [23, 24].

#### A. Unforced Bifurcation Analysis

Consider a general autonomous dynamical system of the form:

$$\dot{\mathbf{x}} = \mathbf{f}(\mathbf{x}, \mathbf{u}) \quad \mathbf{x}, \mathbf{f} \in \mathbb{R}^n \quad (11)$$

where  $\mathbf{f}$  is a vector of  $n$  smooth (differentiable) functions,  $\mathbf{x}$  is the state vector of dimension  $(n \times 1)$  and  $\mathbf{u}$  is the input vector. In the context of open-loop flight dynamics,  $\mathbf{f}$  is usually the equations of motion,  $\mathbf{x}$  is the aircraft's states like  $\alpha, V$ , and  $\mathbf{u}$  contains the control inputs (i.e., elevator, aileron, etc.). The system is in equilibrium when:

$$\dot{\mathbf{x}} = \mathbf{0} \quad (12)$$

Oscillatory solutions, such as a period orbit of period  $T$ , exist when:

$$\mathbf{x}(t) = \mathbf{x}(t + T) \quad (13)$$

By solving equation (12) and/or equation (13), a map of steady states (either equilibrium or periodic) as functions of one of the control inputs in  $\mathbf{u}$  can be generated. This map is referred to as a bifurcation diagram. We solve the equations numerically using continuation methods [25], which utilises a path-following algorithm to traces out a map of solutions as a parameter in  $\mathbf{u}$  is varied. This varying parameter is referred to as the continuation parameter. Numerical continuation requires knowledge of at least one solution, which can be obtained by the user through time-integration method (simulating the system in equation (11) long enough so that the states converge to their final values, assuming the system is stable) or Newton's method for equilibria. In many published works, the terms 'bifurcation analysis' and 'numerical continuation' are used interchangeably.

A bifurcation can be encountered in a nonlinear system, which reflects a qualitative change in the dynamics. Its mathematical definition is:

- For equilibrium solutions: when at least one eigenvalue of the system's Jacobian matrix  $J = df/dx|_{x_0}$  (evaluated at the equilibrium point  $x_0$ ) crosses the imaginary axis.
- For oscillatory solutions: when a Floquet multiplier crosses the unit circle.

Different types of bifurcations can lead to various nonlinear behaviours such as a limit cycle, multiple solutions for the same input, and hysteresis. A simple example of these concepts is provided in appendix A for readers who are new to the topic.

### B. Harmonically-Forced Bifurcation Analysis/Nonlinear Frequency Response

Bifurcation analysis can be implemented on a harmonically-forced system, thereby generating a nonlinear Bode plot for frequency analysis. All ensuing motions are therefore periodic. The method to implement the harmonic forcing term into bifurcation analysis best explained by another simple example. Consider the following second-order nonlinear system:

$$\ddot{x} + c\dot{x} + kx + \epsilon x^3 = A \cos \omega t \quad (14)$$

This is the Duffing equation – a textbook example of nonlinear frequency response. In order to utilise the numerical continuation solver, equation (14) has to be re-written into autonomous first-order form (no  $t$  on the right-hand side). This results in the following fourth-order system:

$$\begin{aligned} \dot{x}_1 &= x_2 \\ \dot{x}_2 &= -kx_1 - \epsilon x_1^3 - cx_2 + Ax_4 \\ \dot{x}_3 &= x_3 + \omega x_4 - x_3(x_3^2 + x_4^2) \\ \dot{x}_4 &= -\omega x_3 + x_4 - x_4(x_3^2 + x_4^2) \end{aligned} \quad (15)$$

where  $x_1 = x$ ,  $x_2 = \dot{x}$ , and  $[x_3, x_4] = [\sin \omega t, \cos \omega t]$  (see the appendix for proof). A nonlinear frequency response is then obtained by setting  $\omega$  as the continuation parameter, resulting in the Bode plot as shown in Fig. 6. Due to the nonlinear term, for  $\epsilon > 0$ , the resonance peak leans to the right and creates a region with multiple solutions and the possibility of hysteresis. This is demonstrated by simulating the system with a chirp signal ( $\omega$  increasing or decreasing linearly). The data from time simulation is then superimposed on Fig. 6, which verifies the jump behaviour and hysteresis predicted by nonlinear frequency analysis.

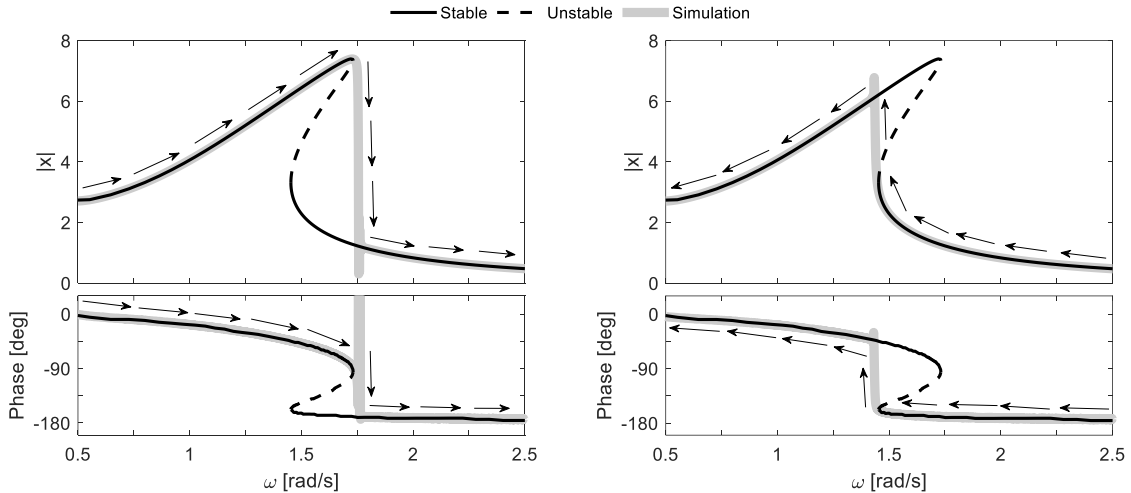


**Fig. 6** Frequency response of the Duffing equation with time simulation data superimposed.  $[c, k, \epsilon, A] = [0.2, 1, 0.05, 2.5]$ .

All bifurcation analysis in this paper was performed using the Dynamical Systems Toolbox [26], which is the MATLAB/Simulink implementation of the numerical continuation software AUTO [27].

## IV. Results and Discussions

We will now compare the flight dynamics characteristics of the NASA GTT using two different aerodynamic modelling methods: quasi-steady and unsteady. In both cases, the following standard fourth-order equations of motion for longitudinal dynamics are used:

$$\dot{\alpha} = \frac{1}{mV} \left[ \frac{1}{2} \rho V^2 S (C_z \cos \alpha - C_x \sin \alpha) - T \sin \alpha + mg \cos(\theta - \alpha) \right] + q \quad (16)$$

$$\dot{V} = \frac{1}{m} \left[ \frac{1}{2} \rho V^2 S (C_z \sin \alpha + C_x \cos \alpha) + T \cos \alpha - mg \sin(\theta - \alpha) \right] \quad (17)$$

$$\dot{q} = \frac{1}{2} \rho V^2 S c \frac{C_m}{I_y} \quad (18)$$

$$\dot{\theta} = q \quad (19)$$

The aircraft parameters are shown in Table 1. The three total aerodynamic coefficients [ $C_x$ ,  $C_z$ ,  $C_m$ ] are made up of static and dynamic components. Table 2 lists the data type for each static coefficient, and Table 3 summarises how the total component was calculated in the quasi-steady and unsteady models.

**Table 1. Aircraft parameters**

$S$	wing area	70.08 m <sup>2</sup>
$c$	mean aerodynamic chord	3.37 m
$m$	mass	25,332 kg
$\rho$	air density (at 10,000 ft)	0.90463 kg/m <sup>3</sup>
$I_y$	pitch moment of inertia	1,510,624 kg m <sup>2</sup>
$T$	thrust	22,000 N
$g$	gravitational acceleration	9.81 m/s <sup>2</sup>

**Table 2. Static aerodynamic data types**

	Quasi-steady	Unsteady ( $\Lambda = 1$ and 2.5)
$C_{x-st}$	Tabular (not shown)	Tabular (not shown)
$C_{z-st}$	Splines (Fig. 2a)	Splines (Fig. 2a)
$C_{m-st}$	Splines (Fig. 2b)	Splines (Fig. 2b)

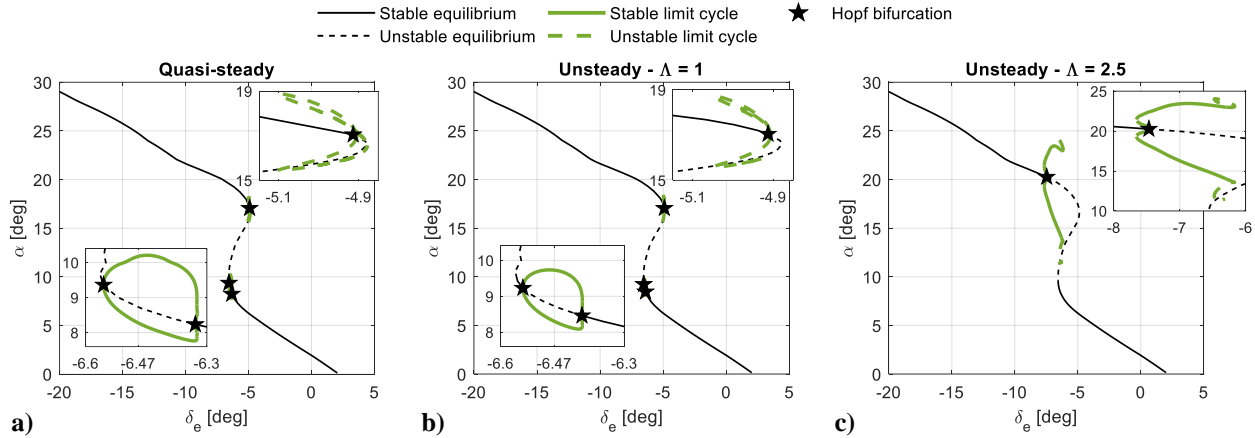
**Table 3. Modelling methods of the three total aerodynamic coefficients**

	Quasi-steady	Unsteady ( $\Lambda = 1$ and 2.5)
$C_x$	Similar to eq. (3)	Similar to eq. (3)
$C_z$	eq. (3)	eq. (7-8)
$C_m$	eq. (4)	eq. (9-10)

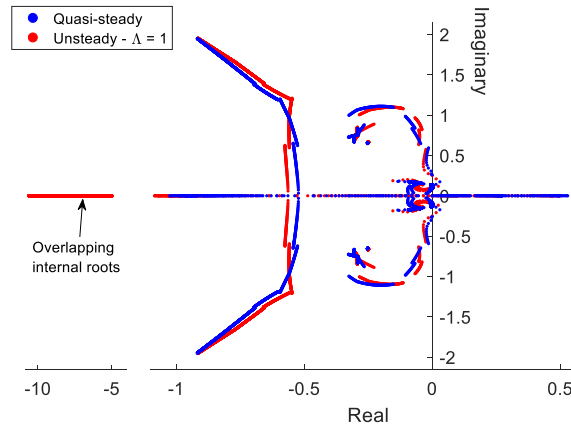
### A. Unforced Bifurcation Analysis

Fig. 7 shows the unforced bifurcation diagrams of the quasi-steady and unsteady GTT with the elevator deflection  $\delta_e$  as the continuation parameter. The insets are magnified views of regions where limit cycles exist. Firstly, it is noted that Figs. 7a and b are very similar and suggest that dynamics of the quasi-steady and nominal-unsteady models are comparable. This observation is further verified in Fig. 8, which compares the pole positions of all equilibrium solutions shown the first two bifurcation diagrams (Figs. 7a and b). The rigid-body roots of the quasi-steady and nominal-unsteady models are comparable, although the latter model contains two additional real roots on the far-left due to the two internal states  $x_z$  and  $x_m$ . These two roots overlap each other and travel as a real pair (as opposed to a

common complex-conjugate pair). Apart from this minor difference, the similar rigid-body roots verify that the state-space method is a valid alternative to quasi-steady modelling while also highlighting that unsteady aerodynamics in the current application (a transport aircraft model that does not undergo rapid manoeuvres) is not sufficiently influential to require a time-dependent model. One can also make an opposite conclusion: that quasi-steady modelling is adequate for the GTT and possibly for any general T-tail transport aircraft applications.



**Fig. 7** Forced bifurcation diagrams – elevator continuation.



**Fig. 8** Pole positions of all equilibrium solutions in Figs. 7a and b.

Figures 7a and b also feature a pair of Hopf bifurcation between  $8.2^\circ$  and  $9.4^\circ$  angle-of-attack. They give rise to a branch of stable limit cycles, meaning that the aircraft may encounter pitch oscillation in the region. This pair of Hopf bifurcations disappears in Fig. 7c when  $\Lambda$  is increased to 2.5. To verify the pitch oscillation, we trim the aircraft at  $\delta_e = -6.3^\circ$ , then step down to  $-6.47^\circ$ . The resulting responses in Fig. 9 verify the limit cycle’s existence in the quasi-steady and nominal-unsteady cases. For the  $\Lambda = 2.5$ , the aircraft is technically stable but is also marginally damped.

Another Hopf bifurcation is detected at a higher angle-of-attack. This occurs at around  $\alpha = 17^\circ$  for the first two cases, resulting in a branch of unstable limit cycles that collides with the unstable equilibrium branch (i.e., a global homoclinic bifurcation). These unstable limit cycles are not directly observable in time simulation. However, the similarity between figures 7a and b further emphasises that quasi-steady modelling is adequate to characterise the dynamics of the aircraft for the current application. When  $\Lambda$  is increased to 2.5, this Hopf bifurcation moves further to the left to reside at a higher angle-of-attack and create a branch of stable limit cycles that can be observed in time simulation – one of which is shown in Fig. 10 alongside a plot of how  $C_M$  varies with  $\alpha$  throughout the oscillation. In the latter, it was found that the oscillation is linked to the damping loop in  $C_M$  being partly undamped, which in turn

was a result of the highly unsteady aerodynamics. In other words, increasing  $\Lambda$  reduces damping at high angles-of-attack, which can lead to stability loss and pitch oscillation in extreme cases.

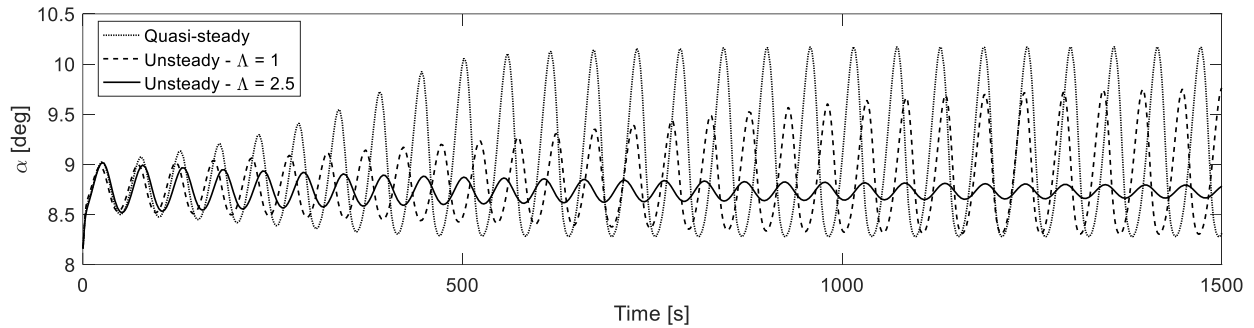


**Fig. 9 Response to an elevator step from  $-6.3^\circ$  to  $-6.47^\circ$ .**

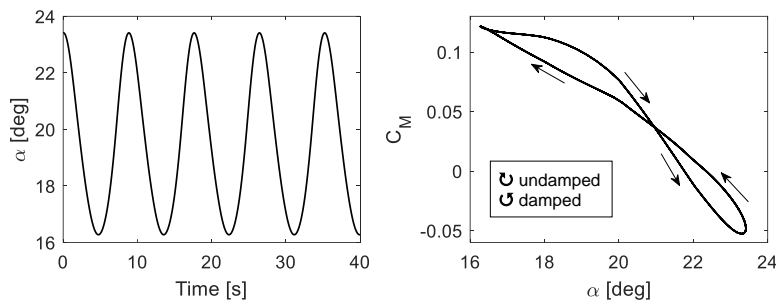


**Fig. 10 A high- $\alpha$  stable limit cycle.  $[\Lambda, \delta_e] = [2.5, -7]$ .**

Finally, the reduced damping at high  $\alpha$  is further highlighted by a large elevator step from  $-2^\circ$  to  $-8^\circ$  (Fig. 11). Based on the bifurcation diagrams, this manoeuvre equates to moving between the two stable trim points at  $3.6^\circ$  and  $20.6^\circ$  angle-of-attack. It can be seen from Fig. 11 that the quasi-steady and nominal-unsteady responses are very similar. On the other hand, the  $\Lambda = 2.5$  case is very different in addition to being significantly less damped as inferred above.

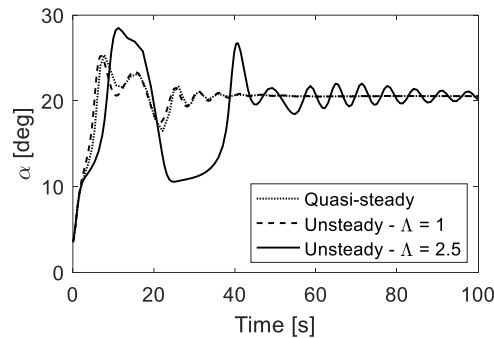


**Fig. 11 Response to an elevator step from  $-2^\circ$  to  $-8^\circ$ .**

In conclusion, unforced bifurcation analysis and time simulations verify that the state-space method provides a feasible alternative to the quasi-steady modelling approach. Conversely, it can also be said that, based on the cases studied here, a quasi-steady model can be considered adequate for transport aircraft applications that do not undergo rapid manoeuvres. On the other hand, the responses become very different in the hypothetical highly-unsteady case, which underline the shortcomings of the quasi-steady method in instances where the unsteady effects are significant. The analyses also demonstrated the potential of combining the state-space modelling method with bifurcation analysis for studying the aircraft's flight dynamics in these highly nonlinear instances.

## B. Forced Bifurcation Analysis

It has been shown that unforced bifurcation analysis provides valuable insights on the effects of unsteady aerodynamics on the aircraft dynamics especially at high angles-of-attack. However, this approach becomes less effective in closed-loop applications in which the controller provides stability. To illustrate this, consider an angle-of-attack-demand system as shown Fig. 12a, where the input is demanded angle-of-attack  $\alpha_d$ . Fig. 12b is the resulting unforced bifurcation diagram of the closed-loop system, which is identical for all three cases (quasi-steady, nominal-unsteady, and highly unsteady). This is because unforced bifurcation analysis only provides information on the equilibrium solutions. Since the controller already provides stability and allows us to trim the aircraft at any angle-of-attack within the elevator deflection range, the influence of unsteady aerodynamics is not noticeable Fig. 12b.

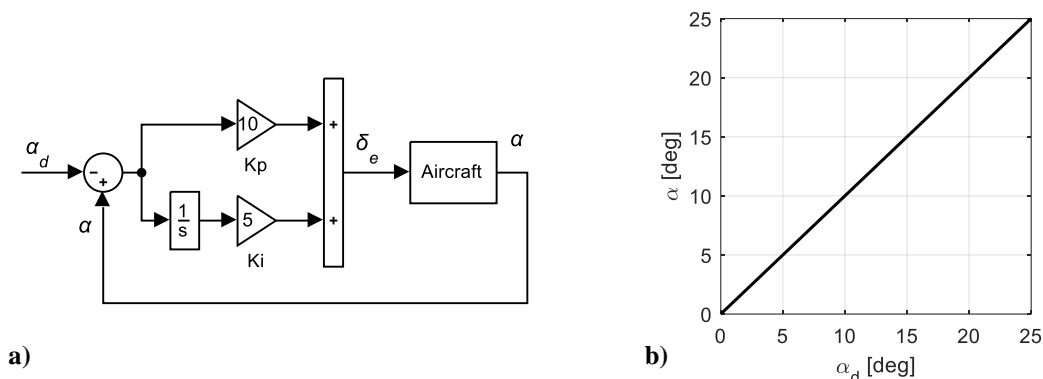


Fig. 12 Closed-loop block diagram (a) and closed-loop unforced bifurcation diagram (b) (same for all cases).

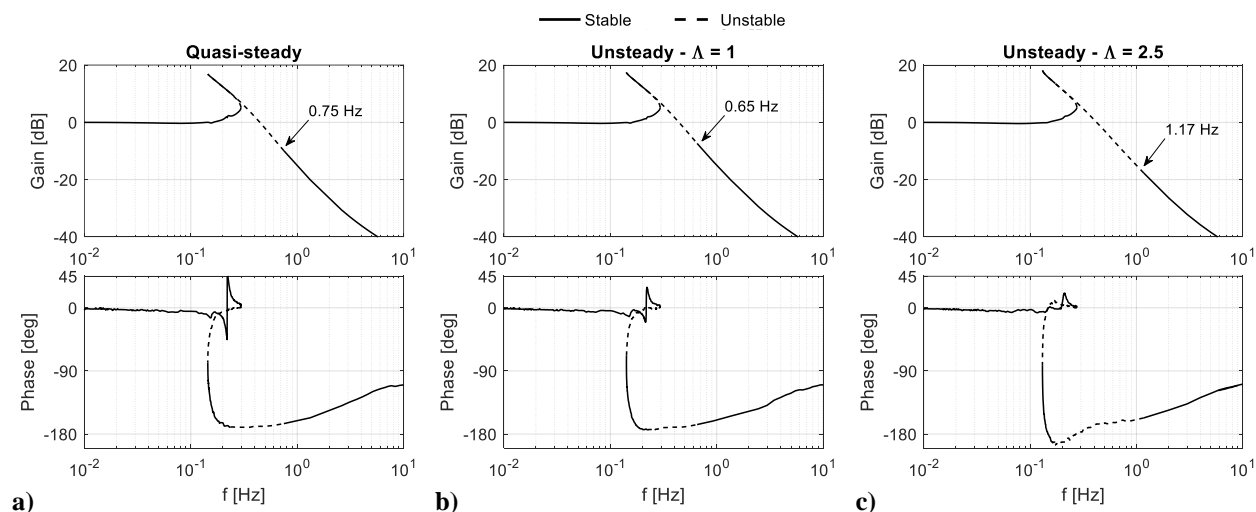
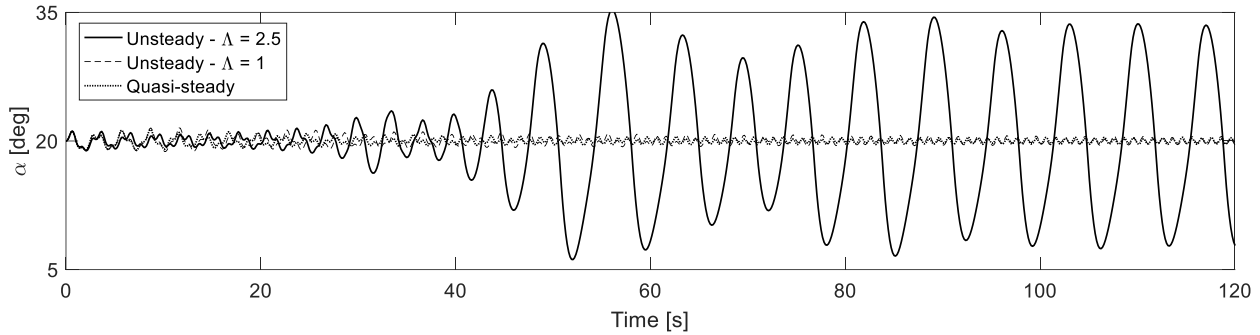


Fig. 13  $\alpha$ -to- $\alpha_d$  frequency responses.  $\alpha_d = 20 + 2 \sin 2\pi ft$  (deg).

In order to assess the controlled aircraft using bifurcation analysis, we will now employ the nonlinear frequency analysis method to observe the impact of the unsteady effects when the aircraft is non-stationary. The pilot input now takes the form  $\alpha_d = 20 + 2 \sin 2\pi ft$  (deg). This is equivalent to trimming the aircraft at  $20^\circ$  angle-of-attack, then apply a forcing input with amplitude  $2^\circ$  and frequency  $f$  (Hz). The resulting Bode plots are shown in Fig. 13. As before, the quasi-steady and nominal-unsteady cases are very similar, and both become unstable for a range of frequencies near resonance below 1 Hz. The resonance peak also includes a region of observable hysteresis; this feature is not discussed further as it is not caused by the unsteady effects. When  $\Lambda$  is increased to 2.5, these unstable solutions increase beyond 1 Hz and only become stable again at 1.17 Hz. In all instances, stability is lost via a torus bifurcation, which gives rise to a large-amplitude quasi-periodic oscillation. We verify this by comparing the forced responses at 1 Hz in time simulation (Fig. 14). As predicted by nonlinear frequency analysis, this high-frequency stick pumping results in very small-amplitude oscillations at exactly 1 Hz for the quasi-steady and nominal-unsteady

responses. However, the  $\Lambda = 2.5$  simulation is remarkably different. In addition to having an extremely large amplitude, the oscillation is quasi-periodic with a significantly lower average frequency than the 1 Hz input. This behaviour marks a degraded controller performance. Since the quasi-periodic (unstable) region expands as  $\Lambda$  increases, it can be said that unsteady aerodynamics can negatively affect the controller's performance in a manner that cannot be detected using the quasi-steady modelling approach and even unforced bifurcation analysis with full unsteady aerodynamics modelling. These shortcomings can be addressed by using forced bifurcation analysis.



**Fig. 14 Forced response at 1 Hz.**

## V. Conclusion

This paper presents one of the first attempts at combining the state-space aerodynamic modelling method with bifurcation analysis for a fixed-wing aircraft, and at extending this to investigate the effects of the aerodynamic modelling on transient behaviour via nonlinear frequency responses generated using numerical continuation. Whilst previous studies were limited to assessments of only aerodynamic characteristics, it has been shown here that the influence of unsteady aerodynamics in the context of dynamics and control can be directly evaluated using bifurcation analysis. Combining the state-space aerodynamic modelling method and bifurcation analysis allows us to verify the following observations that have not been thoroughly assessed previously:

- Quasi-steady aerodynamic modelling is adequate for the NASA GTT model, and potentially more generally for other T-tail transport aircraft that do not undergo rapid manoeuvring.
- Likewise, the state-space modelling approach is a feasible alternative that provides comparable responses in regions where the quasi-steady results are known to be valid.
- When the unsteady effects are significant, the aircraft's open- and closed-loop performance can be severely degraded, especially at high angles-of-attack and while transitioning between the stall and post-stall regimes.

In the hypothetical highly-unsteady study, unforced bifurcation analysis detected the formation of stable limit cycles in the post-stall regime, and harmonically forced bifurcation analysis confirmed the significant reduction in pitch damping via the widened resonance region. Both of these indicate a severely degraded flying qualities caused by the aerodynamic phenomena that cannot be reflected using the traditional quasi-steady modelling technique. Furthermore, the time delay parameters have been chosen to resemble a delta wing configuration found in high-performance fighter aircraft. This suggests that an accurate mathematical model of these highly manoeuvrable platforms must account for unsteady aerodynamic effects in order to accurately represent the stall and post-stall behaviours. To this end, the combination of state-space aerodynamic modelling and bifurcation analysis presents a possible alternative to the traditional quasi-steady method and conventional analysis methods.

## Appendices

### A. An Example of Unforced Bifurcation Analysis

Consider the following simple dynamical system:

$$\ddot{x} + (x^2 - m)\dot{x} + x = 0 \tag{A1}$$

This is a variation of the Van der Pol oscillator. Nonlinearity comes from the damping term  $(x^2 - m)$ . It can be seen that an equilibrium solution exists at the origin, and that increasing  $m$  beyond 0 destabilises this equilibrium point due to the negative damping. Indeed, Fig. A1 shows the time simulation and phase plot at  $m = 1$  with non-zero initial conditions. The system enters a stable self-sustained oscillation that is only suppressed by the increased damping as  $x$  moves away from the origin. Consequently, its phase plot shows a closed-trajectory (i.e., a limit cycle).

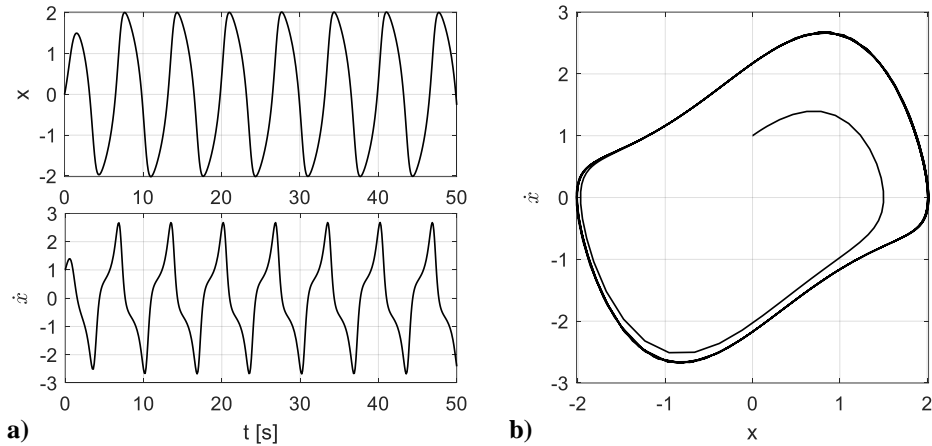


**Fig. A1 Time simulation (a) and phase plot (b) of equation (A1).**

Fig. A2a is the bifurcation diagrams of equation (A1) with  $m$  as the continuation parameter. Stable equilibrium solutions exist for all negative  $m$ . When  $m$  exceeds 0, a Hopf bifurcation is detected, which led to a family of stable limit cycle that increases in amplitude with increasing  $m$  (i.e., damping becomes increasingly negative). The link between the limit cycle amplitude and  $m$  can be verified by running a time simulation with  $m$  reducing linearly from a high value at a rate of  $0.26t$ . Data from this time simulation (plotted in terms of  $m$  rather than  $t$ ) are superimposed on Fig. A2a, which matches the prediction made by bifurcation analysis. The 3D projection of the phase plot is shown in Fig. A2b.

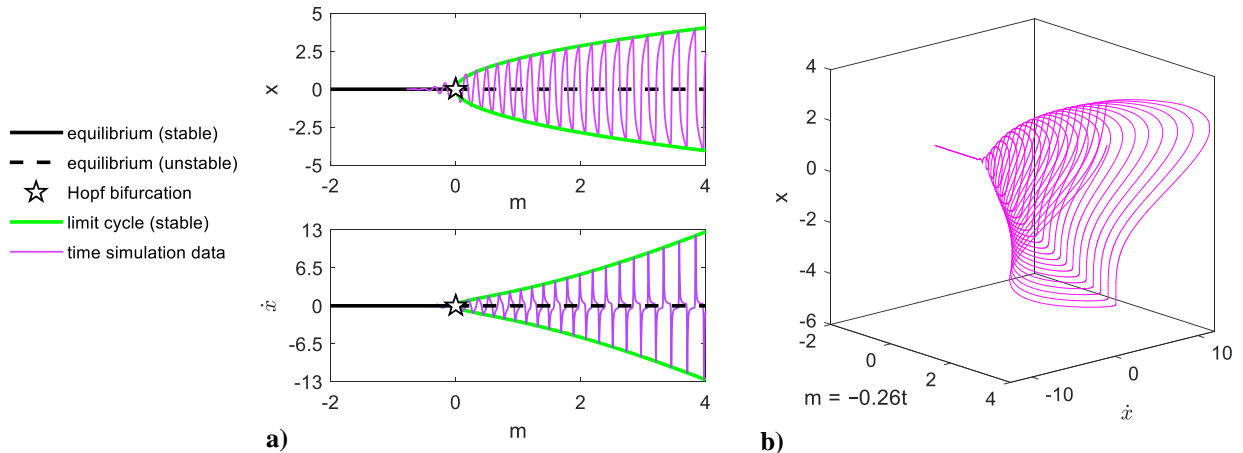


**Fig. A2 Bifurcation diagram of the modified Van der Pol oscillator with simulated response superimposed (a). 3D projection of the simulation data (b)**



## B. Proof of the Harmonic Oscillator Equations

The third and fourth states derivatives in equations (15) are reproduced below:

$$\begin{aligned}\dot{x}_3 &= x_3 + \omega x_4 - x_3(x_3^2 + x_4^2) \\ \dot{x}_4 &= -\omega x_3 + x_4 - x_4(x_3^2 + x_4^2)\end{aligned}\tag{A2}$$

Introducing the complex variable  $z = x_4 + ix_3$ . We have:

$$|z|^2 = x_3^2 + x_4^2\tag{A3}$$

and

$$\begin{aligned}\dot{z} &= \dot{x}_4 + i\dot{x}_3 \\ &= [-\omega x_3 + x_4 - x_4(x_3^2 + x_4^2)] + i[x_3 + \omega x_4 - x_3(x_3^2 + x_4^2)] \\ &= (x_4 + ix_3) - (x_3^2 + x_4^2)(x_4 + ix_3) + i\omega(x_4 + ix_3) \\ &= z - |z|^2 z + i\omega z \\ &= z(1 - |z|^2 + i\omega)\end{aligned}\tag{A4}$$

Now transform  $z$  to its polar form of  $z = re^{i\theta}$ , giving  $|z|^2 = r^2$ . Substitute these in equation (A4):

$$\dot{z} = re^{i\theta}(1 - r^2 + i\omega)\tag{A5}$$

Furthermore, the first derivative of  $z = re^{i\theta}$  is:

$$\dot{z} = \dot{r}e^{i\theta} + i\dot{\theta}re^{i\theta} = e^{i\theta}(\dot{r} + i\dot{\theta}r)\tag{A6}$$

Equating (A5) and (A6) and cancelling  $e^{i\theta}$  gives:

$$r(1 - r^2) + i\omega r = \dot{r} + i\dot{\theta}r\tag{A7}$$

Therefore:

$$\begin{cases} \dot{r} = r(1 - r^2) \\ \dot{\theta} = \omega \end{cases}\tag{A8}$$

It can be seen that  $r = 1$  gives  $\dot{r} = 0$ . In this instance, the system becomes:

$$\begin{cases} \dot{r} = 0 \\ \dot{\theta} = \omega \end{cases}\tag{A9}$$

Which describes a phasor of constant radius 1 and constant angular velocity  $\omega$  rad/s. Its real and imaginary components are  $x_4 = \cos \omega t$  and  $x_3 = \sin \omega t$ , respectively. To ensure that  $r = 1$  at the start of the simulation, set  $x_3(t = 0) = 0$  and  $x_4(t = 0) = 1$ .

We can now couple the states  $x_3$  and/or  $x_4$  into the system's equations of motion to generate the harmonic forcing term in autonomous form for bifurcation analysis.

## Acknowledgments

The first author is partially funded by the University of Bristol's Alumni Grant. The second author is funded by the EU H2020 SAFEMODE project (grant agreement ID: 814961). We are grateful to NASA Langley Research Center, specifically Kevin Cunningham and Gautam Shah, for providing the GTT model aerodynamic data.

## References

1. Bryan, G. H., *Stability in Aviation: An Introduction to Dynamical Stability as Applied to the Motions of Aeroplanes*, chapter II, Macmillan and Company, Limited, London, 1911.
2. Abzug, M. J., and Larrabee, E. E., *Airplane Stability and Control: A History of the Technologies that Made Aviation Possible*, 2, Cambridge Aerospace Series, Cambridge University Press, Cambridge, 2002.  
doi: DOI: 10.1017/CBO9780511607141
3. Abramov, N. B., Goman, M. G., Khrabrov, A. N., and Soemarwoto, B. I. "Aerodynamic Modeling for Poststall Flight Simulation of a Transport Airplane", *Journal of Aircraft*, Vol. 56, No. 4, 2019, pp. 1427-1440.  
doi: 10.2514/1.C034790
4. Goman, M. G., and Khrabrov, A. N. "State-space representation of aerodynamic characteristics of an aircraft at high angles of attack", *Journal of Aircraft*, Vol. 31, No. 5, 1994, pp. 1109-1115.  
doi: 10.2514/3.46618
5. Khrabrov, A., Vinogradov, Y., and Abramov, N. "Mathematical Modelling of Aircraft Unsteady Aerodynamics at High Incidence with Account of Wing-Tail Interaction", *AIAA Atmospheric Flight Mechanics Conference and Exhibit*, AIAA Paper AIAA 2004-5278, 2004.  
doi: 10.2514/6.2004-5278
6. Abramov, N., Goman, M., and Khrabrov, A. "Aircraft Dynamics at High Incidence Flight with Account of Unsteady Aerodynamic Effects", *AIAA Atmospheric Flight Mechanics Conference and Exhibit*, Paper AIAA 2004-5274, 2004.  
doi: 10.2514/6.2004-5274
7. Heller, M., Holmberg, J., and David, R. "Significance of Unsteady Aerodynamic Effects in F/A-18C/D Pitching Moment", *AIAA Atmospheric Flight Mechanics Conference and Exhibit*, AIAA Paper AIAA-2006-6485, 2006.  
doi: 10.2514/6.2006-6485
8. Mehra, R., and Carroll, J. "Bifurcation analysis of aircraft high angle-of-attack flight dynamics", *6th Atmospheric Flight Mechanics Conference*, AIAA Paper 80-1599 1980.  
doi: 10.2514/6.1980-1599
9. Carroll, J. V., and Mehra, R. K. "Bifurcation Analysis of Nonlinear Aircraft Dynamics", *Journal of Guidance, Control, and Dynamics*, Vol. 5, No. 5, 1982, pp. 529-536.  
doi: 10.2514/3.56198
10. Jahnke, C. C., and Culick, F. E. C. "Application of bifurcation theory to the high-angle-of-attack dynamics of the F-14", *Journal of Aircraft*, Vol. 31, No. 1, 1994, pp. 26-34.  
doi: 10.2514/3.46451
11. Guicheteau, P. "Bifurcation theory: a tool for nonlinear flight dynamics", *Philosophical Transactions of the Royal Society of London. Series A: Mathematical, Physical and Engineering Sciences*, Vol. 356, No. 1745, 1998, pp. 2181-2201.  
doi: 10.1098/rsta.1998.0269
12. Kwatny, H. G., Dongmo, J.-E. T., Chang, B.-C., Bajpai, G., Yasar, M., and Belcastro, C. "Nonlinear Analysis of Aircraft Loss of Control", *Journal of Guidance, Control, and Dynamics*, Vol. 36, No. 1, 2013, pp. 149-162.  
doi: 10.2514/1.56948
13. Gill, S. J., Lowenberg, M. H., Neild, S. A., Krauskopf, B., Puyou, G., and Coetzee, E. "Upset Dynamics of an Airliner Model: A Nonlinear Bifurcation Analysis", *Journal of Aircraft*, Vol. 50, No. 6, 2013, pp. 1832-1842.  
doi: 10.2514/1.C032221

14. Rezgui, D., Lowenberg, M. H., Jones, M., and Monteggia, C. "Continuation and Bifurcation Analysis in Helicopter Aeroelastic Stability Problems", *Journal of Guidance, Control, and Dynamics*, Vol. 37, No. 3, 2014, pp. 889-897.  
doi: 10.2514/1.60193
15. Nguyen, D. H., Lowenberg, M. H., and Neild, S. A. "Frequency-Domain Bifurcation Analysis of a Nonlinear Flight Dynamics Model", *Journal of Guidance, Control, and Dynamics*, Vol. 44, No. 1, 2021, pp. 138-150.  
doi: 10.2514/1.G005197
16. Nguyen, D. H., Lowenberg, M. H., and Neild, S. A. "Effect of Actuator Saturation on Pilot-Induced Oscillation: a Nonlinear Bifurcation Analysis", *Journal of Guidance, Control, and Dynamics*, Vol. 44, No. 5, 2021, pp. 1018-1026.  
doi: 10.2514/1.G005840
17. Cunningham, K., Shah, G. H., Hill, M. A., Pickering, B. P., Litt, J. S., and Norin, S. "A Generic T-tail Transport Airplane Simulation for High-Angle-of-Attack Dynamics Modeling Investigations", *2018 AIAA Modeling and Simulation Technologies Conference*, AIAA Paper AIAA-2018-1168, 2018.  
doi: 10.2514/6.2018-1168
18. Cunningham, K., Shah, G. H., Frink, N. T., McMillin, S. N., Murphy, P. C., Brown, F. R., Hayes, P. J., Shweyk, K. M., and Nayani, S. N. "Preliminary Test Results for Stability and Control Characteristics of a Generic T-tail Transport Airplane at High Angle of Attack", *2018 AIAA Atmospheric Flight Mechanics Conference*, AIAA Paper AIAA-2018-0529, 2018.  
doi: 10.2514/6.2018-0529
19. Cunningham, K., Shah, G. H., Murphy, P. C., Hill, M. A., and Pickering, B. "Pilot Sensitivity to Simulator Flight Dynamics Model Formulation for Stall Training", *AIAA Scitech 2019 Forum*, AIAA Paper AIAA-2019-0717, 2019.  
doi: 10.2514/6.2019-0717
20. Williams, D. R., Reißner, F., Greenblatt, D., Müller-Vahl, H., and Strangfeld, C. "Modeling Lift Hysteresis on Pitching Airfoils with a Modified Goman–Khrabrov Model", *AIAA Journal*, Vol. 55, No. 2, 2017, pp. 403-409.  
doi: 10.2514/1.J054937
21. Sedky, G., Jones, A. R., and Lagor, F. D. "Lift Regulation During Transverse Gust Encounters Using a Modified Goman–Khrabrov Model", *AIAA Journal*, Vol. 58, No. 9, 2020, pp. 3788-3798.  
doi: 10.2514/1.J059127
22. Greenwell, D., Khrabrov, A., Goman, M., and Abramov, N. "Two-step linear regression method for identification of high incidence unsteady aerodynamic model", *AIAA Atmospheric Flight Mechanics Conference and Exhibit*, Paper AIAA 2001-4080, 2001.  
doi: 10.2514/6.2001-4080
23. Strogatz, S. H., *Nonlinear Dynamics and Chaos: with Applications to Physics, Biology, Chemistry, and Engineering*, Addison–Wesley, Reading, MA, 1994.
24. Kuznetsov, I. A., *Elements of applied bifurcation theory*, 3rd ed., Applied mathematical sciences ; v. 112, Springer, New York, 2004.
25. Krauskopf, B., Osinga, H. M., and Galán-Vioque, J., *Numerical continuation methods for dynamical systems: path following and boundary value problems*, Understanding Complex Systems, chapter 1, Springer, Dordrecht, 2007.  
doi: 10.1007/978-1-4020-6356-5

26. Coetzee, E., Krauskopf, B., and Lowenberg, M. H. "The Dynamical Systems Toolbox: Integrating AUTO into Matlab", *16th US National Congress of Theoretical and Applied Mechanics*, USNCTAM Paper USNCTAM2010-827, 2010.
27. Doedel, E. J. "*AUTO-07P, Continuation and Bifurcation Software for Ordinary Differential Equations, Ver. 07P*", <http://www.macs.hw.ac.uk/~gabriel/auto07/auto.html> [retrieved 8 April 2021].